IEEE Access
Multidisciplinary | Rapid Review | Open Access Journal

Received October 9, 2018, accepted October 25, 2018, date of publication October 31, 2018,
date of current version December 27, 2018.

Digital Object Identifier 10.1109/ACCESS.2018.2878941

A High-Selective Frequency Selective Surface With Hybrid Unit Cells

YUHONG MA, WEIWEI WU, YE YUAN, WENTAO YUAN, AND NAICHANG YUAN
State Key Laboratory of Complex Electromagnetic Environment Effects on Electronics and Information System, National University of Defense Technology, Changsha 410000, China

Corresponding author: Weiwei Wu (shirleysp1130@hotmail.com)

This work was supported by the National Natural Science Foundation of China under Grant 61302017.

ABSTRACT In this paper, a novel frequency selective surface (FSS) is proposed. It has two metal layers and the configurations of the unit cells of these two layers are different, so-called hybrid unit cells. The designed FSS has three transmission zeros and steep roll-offs at the edges of the passband. In our design process, the top layer is used to achieve two transmission zeros at the edges of passband and the bottom layer is used to achieve wideband performance and transmission zero at the right side of the passband. The effects of the geometrical parameters on the frequencies of transmission poles and zeros are analyzed. By establishing an equivalent circuit, the matching impedance network is obtained quickly by Microwave Office and the flatness and insertion loss of the passband are improved after introducing the matching impedance network. The prototype of the proposed FSS is manufactured and tested. The measured −1.5-dB passband is from 13.2 to 19 GHz, and its relative bandwidth can achieve 36%. The measured results verify the design. This FSS is a good candidate to strengthen the performances of *Ku*-band satellite and *Ku*-band active radar.

INDEX TERMS Frequency selective surfaces, electromagnetic analysis, equivalent circuit, hybrid unit cells, steep roll-off, wideband.

I. INTRODUCTION

FSSs are two-dimensional or three-dimensional structures, which achieve transmissions of electromagnetic waves in the passbands, absorptions in the absorptive bands and reflections in the stop bands [1]–[9]. With the rapid developments of wireless communication technology, multi-band, broad band and high out-of-band rejection technologies draw a lot of attractions. Some designs are developed to meet the requirements.

There have been a great number of studies in wideband FSSs.

1) The fractal structures transformed by the basic units have different sizes, and the resonance frequency points generated by them will also be different. The reasonable adjustments of the structures enable multiple or broad band working bands [10], [11].
2) Another effective way to achieve wideband FSS is combining multi-layers with different cell units. The FSS with five dielectric substrate layers and four metal layers are analyzed in [12]. A frequency selective surface consisting of a patch array, a lattice array and a medium layer has wideband performance [13]. A novel wideband, low-profile and second-order miniaturized band-pass frequency selective surface (FSS) consisting of metallic mesh and its complementary structures is discussed in [14]. A compact FSS with ultra-wideband bandpass function is presented in [15]. This FSS is a three layer structure composed of three metal layers separated by two dielectric substrates and its measured −3dB bandwidth is from 6.0 to 19.25 GHz. In [16], a low-profile third-order wideband FSS with a thickness of $\lambda/24$ and light weight is studied, and it is composed of resonant and non-resonant elements.
3) Beside above two ways, there are some other ways to achieve wideband performance. A novel FSS with arrays of subwavelength capacitive patches and inductive wire grids not only provides wideband selectivity but also serves as linear-to-circular polarization converter [17]. A novel FSS with a two-dimensional periodic array of microstrip lines has wideband response which is achieved by applying higher-order modes of the array [18].

High out-of-band rejection is achieved by introducing transmission zeros at desired finite frequencies and many efforts have been made.

1) Elements with different working modes are introduced to achieve high selectivity. A three-dimensional

bandpass FSS with multiple transmission zeros is achieved by connecting microstrip lines with ground through metallic vias [19]. Metallic vias can introduce additional resonators provided by the air mode, so the FSS can provide more transmission zeros in the operating band which lead to wide out-of-band rejection. Different operating modes of SIW cavities are also used to accomplish high selectivity FSSs [20], [21].

2) Multiresonant structures are capable of providing high selectivity performance. The FSS with two transmission zeros applies aperture-coupled resonators (ACRs) to realize a high-selectivity at 60 GHz [22].
3) Cascading periodic structures with inductive, capacitive, or resonant type surfaces can also be used to accomplish the high-selective FSS. Combining complementary square loops and meandering slots is used to achieve three transmission poles and two transmission zeros in the frequency response of the FSS [23], [24]. Cascading multi-layer periodic arrays of novel resonant unit cells can achieve high-selective characteristic and improve the out-of-band rejection [25]–[27].

In this paper, we propose a high-selective hybrid dual-layer FSS. This FSS has two metal layers. One metal layer is used to realize wideband characteristic in our design, and the other metal layer is used to add two transmission zeros. The unit cells for these metal layers are different, which means it has hybrid unit cells. In our proposed FSS, the air layer is introduced to improve the flatness and insertion loss of the passband. Simulation results show that this proposed FSS has wideband frequency bands, low loss and steep roll-off at the edges of the passband. Commercial software HFSS and Microwave Office are used to simulate the model.

II. FSS DESIGN PROCESS AND THE MODULATION OF DIFFERENT LAYERS FOR OPTIMIZATION DESIGN

A. THE DESIGN PROCEDURE

The second resonant frequency of the hexagon ring is three times of the fundamental resonant frequency, which has broader passbands compared with other shape rings [4]. The proposed bottom layer is a periodic structure whose unit cell is combined with a hexagon patch and hexagon rings, so-called patch-ring unit cell. In Fig. 2(a), one metal layer with the patch-ring unit cell configuration is simulated. The transmission coefficient of the patch-ring unit cell has wideband performance and a steep roll off at the right side of its passband, but the left side of its passband does not performe well. The transmission and reflection coefficients of one single layer with Jerusalem metal ring configuration obtained by the full-wave simulation and the circuit approach are shown in Fig. 2(b). According to Fig. 2(b), the refelection coefficient of Jerusalem metal ring has two sharp stopbands but the bandwidth of the second stopband is smaller than the one of the first stopband. Jerusalem metal ring is applied to replace one layer of the patch-ring layer. The simulated transmission and reflection coefficients of the final hybrid configuration without an air layer are shown in Fig. 2(c). Then, the air layer is introduced to further improve the performance of this structure. This method can not only reduces insertion loss and smooths the transmission coefficient efficiently, but also reduces the weight of the entire structure. Fig. 2(d) shows the simulated transmission coefficient of our design. The simulated −1.5dB passband of our design is from 13.1GHz to 19.5GHz, and its relative bandwidth can achieve 36%. There are two transmission zeros at frequencies of 10.1GHz and 21.25GHz.

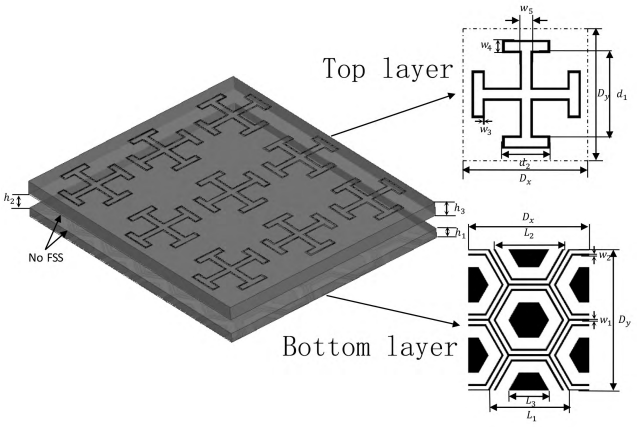

FIGURE 1. FSS unit structure.

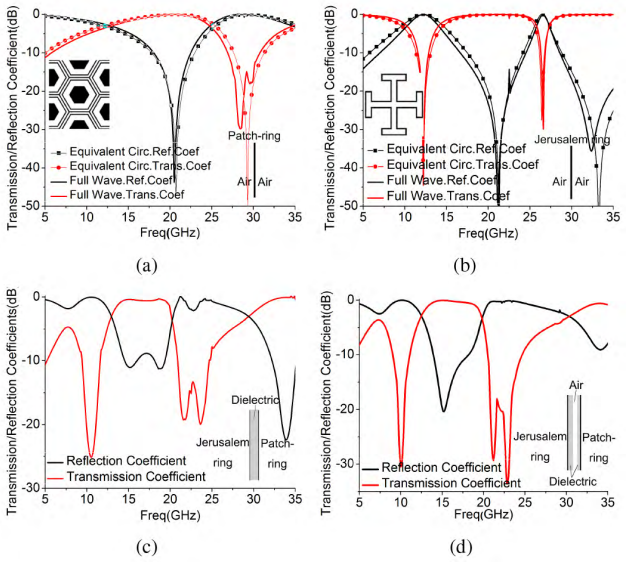

FIGURE 2. Transmission and reflection coefficients of different unit cells, (a) patch-ring unit cell; (b) Jerusalem metal ring unit cell; (c) Jerusalem metal ring unit cell and patch-ring unit cell supported by a dielectric layer; (d)our design.

Fig. 1 shows the design of the FSS unit structure. Its physical parameters are shown in Tab. 1. The air layer is between two dielectric layers. Each metal layer is etched on one dielectric layer. The thickness of the top dielectric

TABLE 1. Physical parameters of the proposed FSS.

Parameter	Value (mm)	Parameter	Value (mm)	Parameter	Value (mm)
D_x	6	L_1	3.9	w_3	0.1
D_y	6.9	L_2	3.5	w_4	0.6
h_1	0.7	L_3	2	w_5	0.6
h_2	1.3	w_1	0.087	d_1	4
h_3	1	w_2	0.087	d_2	2.2

substrate is 1mm and the one of the bottom dielectric substrate is 0.7mm. F4BM-2 is used as the dielectric medium, with a relative permittivity of 2.2, and a loss tangent of 0.0007. The thickness of air layer sandwiched between two dielectric layers is 1.3mm.

B. THE ANALYSES OF THE TOP AND BOTTOM LAYERS

The equivalent circuit of the FSS has been thoroughly studied in [28]–[34]. Although the lumped elements are corresponded with physical structures, the value of lumped element is not completely specified by the single structure and the adjustment of single structure can change values of other lumped elements in the same layer. The sensitivities of the transmission zeros and poles to which parameters of the structure are analyzed by full-wave simulation in this section.

We firstly study the top layer. The function of the top layer is to introduce two transmission zeros, so we pay close attention to its transmission zeros in the process of analyzing. According to the theory of Munk [4], even harmonics can be excited in the ring unit such as the Jerusalem metal ring while the length of unit cell equals to the half a wavelength. The first-order odd mode is excited while the wavelength of the electromagnetic wave equals to the length of the unit cell. So the frequency of the second transmission zero is about double of the one of the first transmission zero. The perimeter of the used Jerusalem ring is 14mm, and the frequency of the first transmission zero is 12.5GHz whose half-wavelength is 12mm. They are almost equivalent. When the geometrical parameters are varied, the frequencies of these two transmission zeros are changed in different tendencies. The relationships between geometrical parameters and the frequencies of two transmission zeros are shown in Fig. 3.

Observe that for the increases of d_1 and d_2, the frequencies of the first and second transmission zeros increase and the increment of the second transmission zero is about double of the increment of the first transmission zero. With the increase of w_3, the gap between the first and second transmission zeros gets wider. While w_4 and w_5 increase, the first transmission zero does not change and the second transmission zero moves to higher frequency point. According to the effects of different values of geometrical parameters on the transmission coefficients, we can flexibly adjust the frequencies of these two transmission zeros.

The bottom layer is used to provide transmission pole and steep-roll in the right of the passband, so its first transmission pole and transmission zero are concerned. The transmission

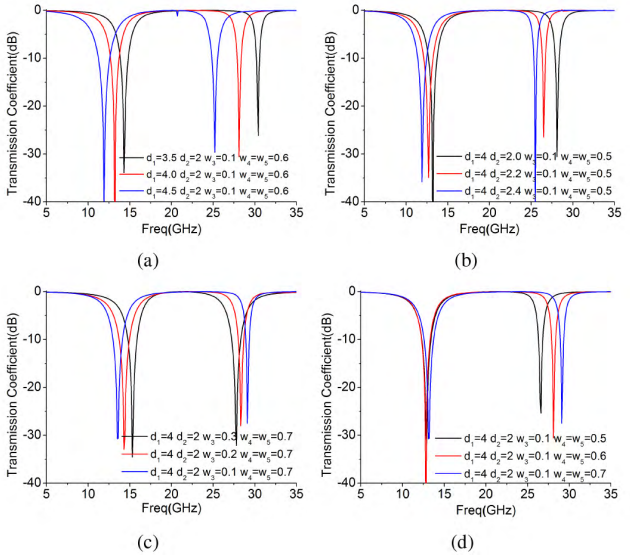

FIGURE 3. Effects of different values of geometrical parameters on the transmission coefficient for the top layer.

pole is generated by the resonance of the aperture between the external hexagonal grid and the internal hexagonal ring. While the perimeter of the internal hexagonal ring equals to the wave length, a transmission pole is generated. The relationships between geometrical parameters and the frequencies of transmission pole and zero are shown in Fig.4.

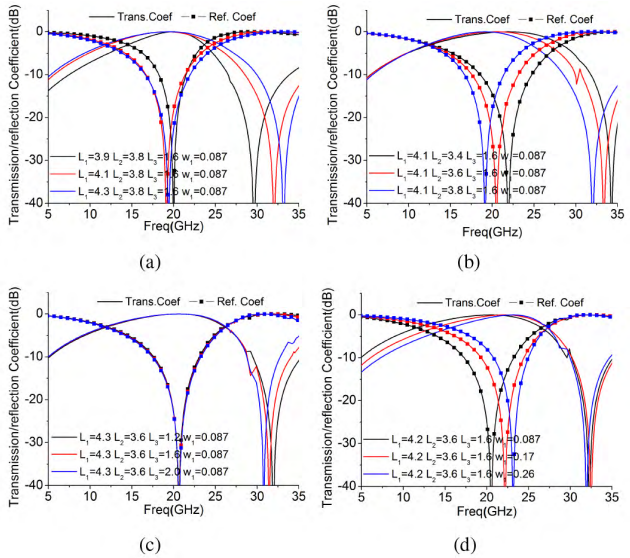

FIGURE 4. Effects of different values of geometrical parameters on the transmission coefficient for the bottom layer.

The frequency of the transmission zero increases with the increase of L_1, while the frequency of transmission pole does not change and the bandwidth of transmission pole increases. For the increase of L_2, the frequencies of transmission pole and zero increase. Increasing the side length of patch L_3 results in the decrease of the transmission zero and the transmission pole does not change. The increase of w_1 does not

affect the transmission zero but results in the increase of the frequency of the transmission pole. Effects of different values of geometrical parameters on the transmission coefficient for the bottom layer shown in Fig.4 guide us in the design and optimization processes.

C. PROPOSED EQUIVALENT CIRCUIT MODEL AND THE PROCESS OF DETERMING THE IMPEDANCE MATCHING NETWORK OF THE BOTTOM AND TOP LAYERS

In above section, the sensitivities of three transmission zeros and one transmission pole to geometrical parameters are presented. In this section, a quick way to improve the flatness and insertion loss of passband is introduced. According to theory of transmission lines, the poor impedance matching of the top layer and bottom layer will cause poor performance. Unlike the traditional way of placing a dielectric layer directly, we add the air layer to the model to achieve proper impedance matching. Equivalent circuits are introduced to determine thicknesses of the air and dielectric layers.

We firstly study the equivalent circuit of the top and bottom layers without loading the dielectric layer.

In [28], the equivalent circuit of a simple cross-metal ring model is shown in Fig. 5(a). Noted that on the top layer, ring structures are added to the four ends of the cross-metal ring model to form a Jerusalem ring unit cell, which introduces the shunt capacitors C_{s_1}. This shunt capacitance C_{s_1} will make the unit size smaller and increase the bandwidth. The equivalent circuit of the top layer is shown in the Fig. 5(b).

The impedance of the proposed equivalent circuit is

$$Z_{FSS} = \frac{(L_{s_1}C_{s_1}L_{p_1}C_{p_1} + 2L_{s_1}C_{s_1}L_{p_1}C_{p_1}C_1)\omega^4}{jC_1\omega(1 - L_{s_1}C_{s_1}\omega^2)(1 - L_{p_1}C_{p_1}\omega^2)} \times \frac{-(L_{s_1}C_{s_1} + L_{p_1}C_{p_1})(1 + C_1)\omega^2 + 1}{jC_1\omega(1 - L_{s_1}C_{s_1}\omega^2)(1 - L_{p_1}C_{p_1}\omega^2)} \quad (1)$$

According to the theory of transmission lines, the transmission coefficient of the proposed FSS is calculated by

$$T(w) = \frac{2Z_{FSS}}{2Z_{FSS} + Z_0} \quad (2)$$

While $Z_{FSS} = \infty$ and $T(w) = 1$, there exists a transmission pole. While $Z_{FSS} = 0$ and $T(w) = 0$, there exists a transmission zero. Once the transmission poles, zeros and the equivalent circuit of the FSS are given, the element values of the equivalent circuit can be determined by the following formula

$$\begin{aligned} C_{s_1} &= \frac{1}{L_{s_1}(w_{p1}^{top})^2}, \\ C_{p_1} &= \frac{1}{L_{p_1}(w_{p2}^{top})^2}, \\ C_1 &= 1/2\left(\frac{1}{L_{s_1}C_{s_1}L_{p_1}C_{p_1}w_{s1}^{top}w_{s2}^{top}} - 1\right). \end{aligned} \quad (3)$$

where w_{s1}^{top} and w_{s2}^{top} respectively represent the frequencies of transmission zeros, and w_{p1}^{top} and w_{p2}^{top} represent the frequencies of transmission poles of the cross-metal ring.

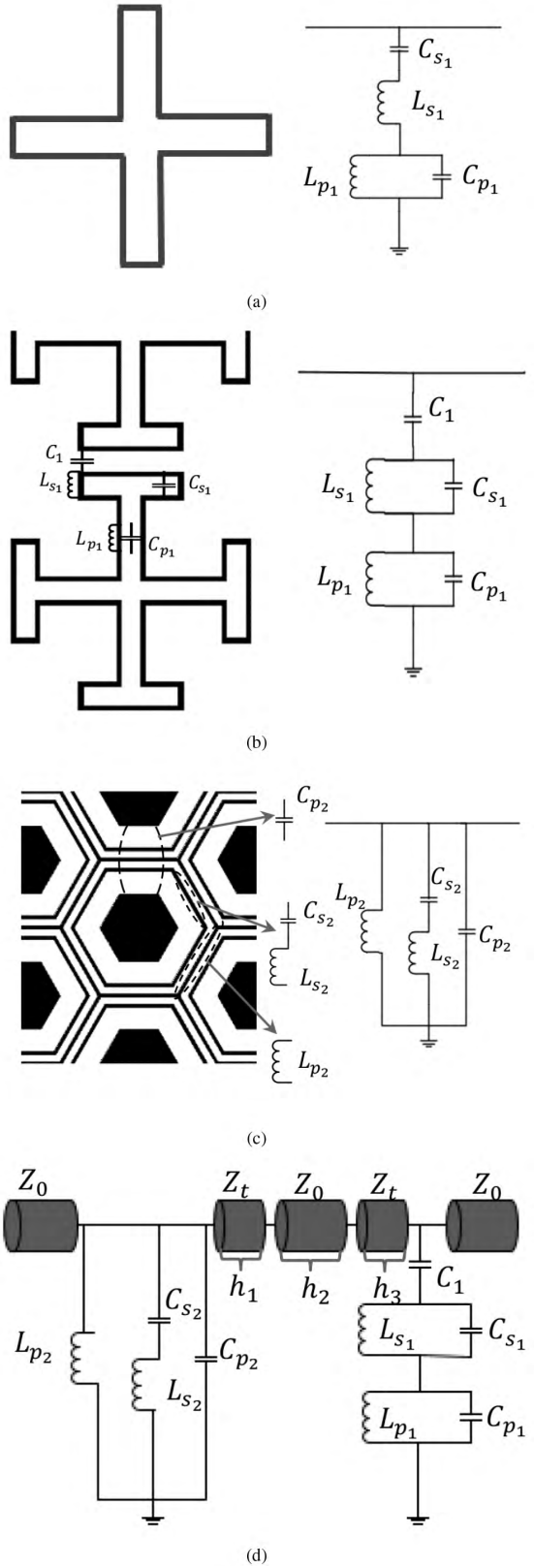

FIGURE 5. The equivalent circuits of the FSS, (a) A simple cross-metal ring; (b) The top layer; (c) The bottom layer; (d) The entire structure.

Eq3 can make sure the transmission zeros and poles of the equivalent circuit are consistent with the ones calculated by the HFSS. To get accurate lumped-LC parameters, we build

an equivalent-circuit model in Microwave Office. L_{s_1} and L_{p_1} are two inductances to tune transmission coefficient of the equivalent circuit simulation. The values of other lumped elements are obtained by the Eq3 while the values of two inductances L_{s_1} and L_{p_1} are given. Then, the values of L_{s_1} and L_{p_1} are tuned until two stopband bandwidths obtained by the equivalent circuit are consistent with two stopband bandwidths obtained by the full-wave simulation. The transmission and reflection coefficients obtained by the circuit approach are shown in Fig. 2(b). They agree well with the results obtained by the full-wave simulation approach.

The equivalent circuit of the bottom layer is shown in Fig. 5(c). The interior hexagonal patch is modeled as C_{p_2} and the external hexagonal grid is modeled as L_{p_2}.The series LC circuit (L_{s_2} and C_{s_2}) represents the internal hexagonal ring. The impedance of the proposed equivalent circuit is

$$Z_{FSS} = \frac{(1 - L_{p_2}C_{p_2}\omega^2)(1 - L_{s_2}C_{s_2}\omega^2) - L_{p_2}C_{s_2}}{jL_{p_2}\omega(1 - L_{s_2}C_{s_2}\omega^2)} \quad (4)$$

To get the lumped parameters of the equivalent circuit, Eq5 are introduced to describe the relationship between lumped elements.

$$\begin{aligned} L_{s_2} &= \frac{1}{C_{s_2}w_{p_1}^{bot^2}}, \\ L_{p_2} &= \frac{(w_s^{bot^2} - w_{p_2}^{bot^2})(w_s^{bot^2} - w_{p_1}^{bot^2})}{-C_{s_2}w_{p_1}^{bot^2}w_{p_1}^{bot^2}w_{p_2}^{bot^2}}, \\ C_{p_2} &= \frac{(w_{p_2}^{bot^2} - w_s^{bot^2}) - C_{s_2}L_{p_2}w_{p_1}^{bot^2}w_{p_1}^{bot^2}w_{p_2}^{bot^2}}{L_{p_2}w_{p_1}^{bot^2}(w_s^{bot^2} - w_{p_1}^{bot^2})}. \end{aligned} \quad (5)$$

Where $w_{p_1}^{bot}$ and $w_{p_2}^{bot}$ respectively represent the transmission poles of the bottom layer and w_s^{bot} represent the transmission zeros of the bottom layer. C_{s_2} is a capacitance to tune transmission coefficient of the equivalent circuit simulation. The values of other lumped elements are obtained by the Eq5 while the value of capacitance C_{s_2} is given. The value of C_{s_2} is tuned until the passband bandwidth obtained by the equivalent circuit is consistent with the one obtained by the full-wave simulation. We use Microwave Office to optimize the values of lumped components until the transmission curve of the equivalent circuit fits well with transmission curve obtained by full-wave simulation.

In the equivalent circuit, the air layer is considered as a transmission line whose length is the same as the thickness of the air layer and its impedance is $Z_0 = 377\Omega$. The dielectric layer is equivalent to another transmission line whose length equals to the thickness of the dielectric layer and its impedance is $Z_t = Z_0/\sqrt{\epsilon_r}$. The equivalent circuit of the entire structure is shown in Fig. 5(d). The equivalent circuit parameters for the top and bottom layers are shown in Tab. 2.

We use Microwave office to simulate the equivalent circuit of the proposed FSS shown in Fig.2(d), and the values of the length of transmission lines are tuned to achieve proper impedance matching. According to [4], for unilateral substrate loading, when the substrate thickness increases from zero to a small value (typically $0.05\lambda_\epsilon$), a steep roll-off of the resonant frequency shows out. As the thickness of the dielectric layer is larger than $0.05\lambda_\epsilon$, the resonant frequency of the FSS continues to decrease and approaches $f_0/\sqrt{(\epsilon_r + 1)/2}$. The transfer curve obtained by the equivalent circuit needs to be divided by the coefficient $\sqrt{(\epsilon_r + 1)/2}$ to compensate the frequency deviation caused by introducing the dielectric layer. After compensating the frequency deviation, the frequency responses of the equivalent circuit for different lengths of the transmission lines obtained by Microwave Office are consistent well with the frequency responses of the FSS for different thicknesses of the air and dielectric layers obtained by HFSS as shown in Fig. 6. The above results show that the thicknesses of the air and dielectric layers obtained by the equivalent circuit simulation are reliable. The coupling between the top and bottom layers is not concerned in the equivalent circuit and the simulation results shows that it does not affect the effectiveness of the method mentioned above.

TABLE 2. The equivalent circuit parameters of the proposed FSS. Capacitor values are in pF and inductor values are in nH.

The equivalent circuit parameter	C_1	L_{s_1}	L_{p_1}	C_{s_1}	C_{p_1}
value	0.0288	1.75	2.36	0.0128	0.022
The equivalent circuit parameter	L_{s_2}	L_{p_2}	C_{s_2}	C_{p_2}	
value	2.69	1.9	0.012	0.009	

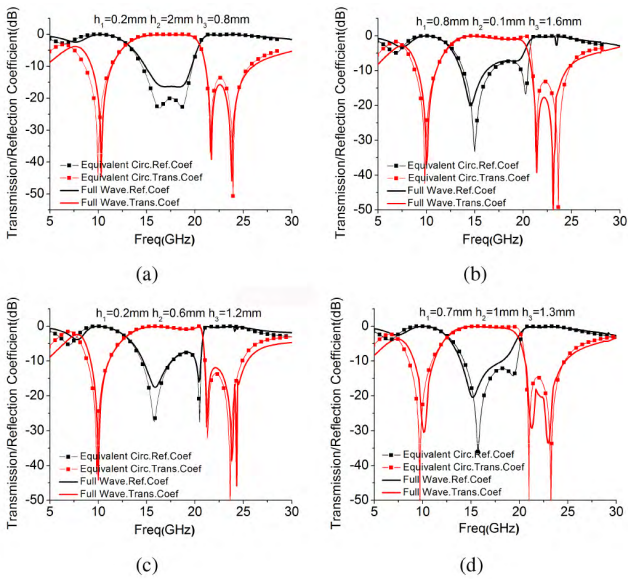

FIGURE 6. Transmission and reflection coefficients of the proposed FSS obtained by full-wave and the equivalent circuit simulation for different thicknesses of the air and dielectric layers.

A lot of efforts and times are saved in the equivalent circuit simulation since the full-wave simulation is quite time-consuming and blind to optimize structure. By using HFSS to perform the full-wave simulation, the simulation of a single layer FSS structure without loading the dielectric

layer will spend 2 to 3 minutes, and entire FSS structure simulation takes more than 15 minutes. For parametric sweeps, the full-wave simulation takes several or several tens of hours. By using Microwave office, we can directly determine the thicknesses of air and dielectric layers which achieve proper impedance matching of the top and bottom layers.

D. THE DESIGN PROCESS

The design of the desired FSS is performed through the following process.

1) Firstly, we make sure the desired frequencies of transmission poles and zeros, and we assign the transmission poles and zeros to the bottom layer and top layers.
2) Then, we determine the approximate geometrical parameters of the top and bottom layers and the relative dielectric constant of the used dielectric layer. For example, the desired transmission pole of the bottom layer is 10GHz and the relative dielectric constant of the dielectric layer is 2.2. After considering the frequency deviation caused by introducing the dielectric layer, the frequency of transmission pole is 12.6GHz, so the side length of the internal hexagonal ring of the designed bottom layer L_2 is about 6mm.
3) The structures of the top and bottom layers are tuned separately under the guide of Sec. II-B by full-wave simulation to make sure the desired frequencies of the transmission zeros and poles.
4) The air and dielectric layers are introduced to achieve impedance matching of the top and bottom layers. The thicknesses of the air and dielectric layers do not affect the frequencies of transmission zeros. So we can only consider which matching impedance network improves the flatness and insertion loss of the passband properly. We obtain the equivalent circuits for the top and bottom layers by the procedure of Sec. II-C and the matching impedance network is obtained quickly by Microwave office. After obtaining the lengths of the transmission lines in the previous step, the thicknesses of the air and dielectric layers are determined.
5) The optimal design is performed afterwards. The adjustment of relevant geometrical parameters can be achieved quickly in the optimization of the transmission zeros and poles by guides of Sec. II-B and Sec. II-C. If the transmission poles or zeros are tuned, we can redesign the matching impedance network by step 4.

III. EXPERIMENTAL VERIFICATION

Using photolithography technology, the FSS prototype with a dimension of $130 \times 127.78mm^2$ is fabricated. The top layer has 20×17 cells and the bottom layer has 34×39 cells. Both of them are etched on the F4BM-2 substrates as shown in Fig. 7. The far-field measurement is used to test the transmission performance of this FSS, as shown in Fig. 8. A pair of horn antennas are used as transmitting and receiving antennas respectively, and the FSS prototype is placed in the free space to measure the effects of the FSS.

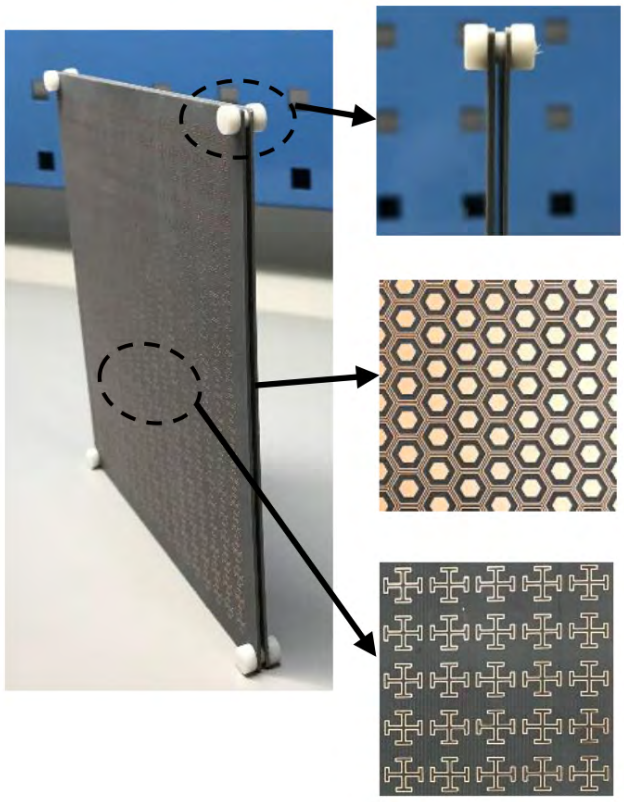

FIGURE 7. Prototype of FSS.

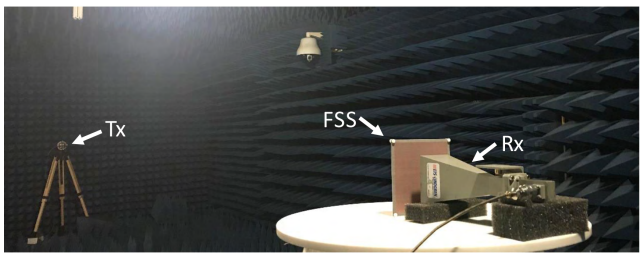

FIGURE 8. Testing setup.

Fig. 9(a) shows the comparison between the equivalent circuit simulation, the full-wave simulation and the actual measurement results of our design, and we can see that both the results of the equivalent circuit and full-wave simulations are in good agreement with the result of physical measurements. The measured $-1.5dB$ passband is from 13.2GHz to 19GHz, and its relative bandwidth can achieve 36%. The measured transmission curve has two transmission zeros and steep roll-offs at the edges of the passband. The measured results show that the proposed design method is feasible and effective.

As a spatial filter, FSS is not only valued by its transmission characteristics under its normal incidence, and its polarization and incident angle stabilities should be concerned as well.

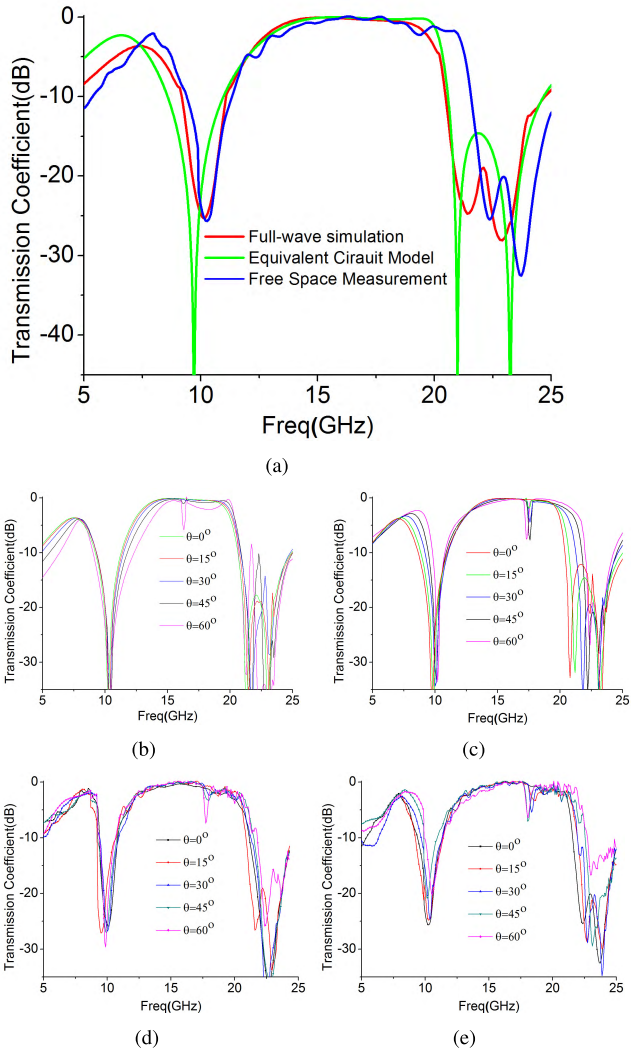

FIGURE 9. Simulated and measured transmission coefficients of the FSS, (a) The transmission coefficients for the TEM (b) The simulated transmission coefficients under various incident angles for the TE; (c) The simulated transmission coefficient under various incident angles for the TM. (d) The measured transmission coefficients under various incident angles for the TE; (e) The measured transmission coefficient under various incident angles for the TM.

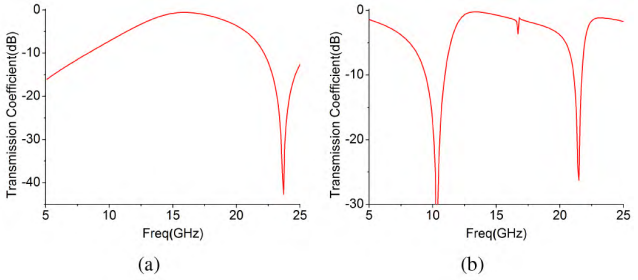

FIGURE 10. The transmission coefficients of the bottom and top layers under incident angle of 60^o (a) the bottom layer; (b)the top layer.

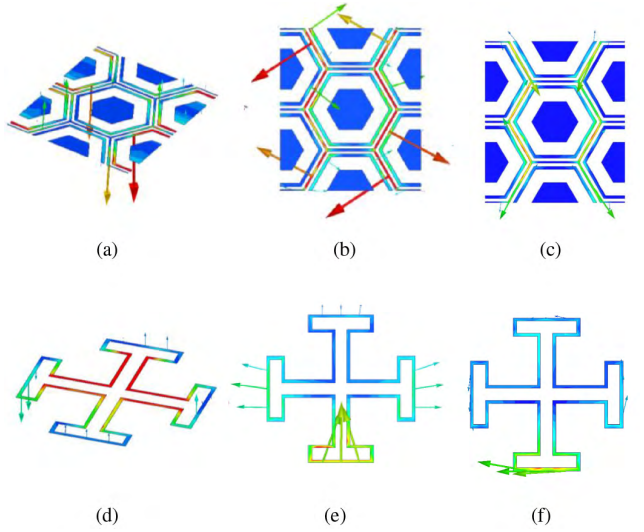

FIGURE 11. The E-field, H-field and current distributions of the top and bottom layers in the frequency of the dip point, (a) The E-field distribution of the bottom layer; (b) The H-field distribution of the bottom layer; (c) The current distribution of the bottom layer; (d) The E-field distribution of the top layer; (e) The H-field distribution of the top layer; (f) The current distribution of the top layer.

The simulated transmission coefficients of the designed FSS under different polarizations and incident angles are shown in Fig. 9(b) and Fig. 9(c). The measured effects of different polarizations and incident angles on the FSS transmission curve are shown in Fig. 9(d) and Fig. 9(e).

When the incident angle exceeds 45 degrees, a dip in the frequency of 16.3GHz occurs in the pass-band regardless of TE wave or TM wave. According to [28], when oblique incident electromagnetic wave strikes the FSS, the equivalent circuit and the values of the lumped elements of the FSS will change, and new resonance point will generate. Then, we individually analyze the top and bottom layers to figure out the causes of dip point. The simulated transmission coefficients of the bottom and top layers under the incident angle of 60^o are shown in Fig. 10. We can come to the conclusion that this dip is caused by the resonance of the top layer. The E-field, H-field and current distributions of the top and bottom layers in the frequency of the dip point is shown in Fig. 11. According to Fig. 11, the oblique incidence of electromagnetic wave generates new pattern in the top layer. According to Fig. 10, the transmission coefficient of bottom layer is affected as well while incident wave is oblique, The current distribution of bottom layer in the frequency of dip point indicates that incident waves arouses in-phase current in the hexagon ring.

Rectangle coefficient is used to describe the steepness of the filter response curve near the cutoff frequency in filter design, and the value of rectangle coefficient is the ratio of −3dB bandwidth to −60dB bandwidth. The higher the value of rectangle coefficient, the FSS has better selective performance. In this article, we define the rectangle coefficient as the ratio of −3dB bandwidth to the bandwidth between two transmission zeros. A comparison between our FSS and other FSSs with two (or more) transmission zeros is shown in Tab 3. It can be found that the proposed FSS has stable wideband

TABLE 3. Comparison of the proposed FSS and other FSSs with two (or more) transmission zeros.

Ref	The working center frequency (GHz)	-3dB bandwidth (GHz)	-3dB bandwidth(TE) (incident angle)	-3dB bandwidth(TM) (incident angle)	Rectangle coefficient	Insertion loss(dB)
[19]	8.2	$B = 1.4$	1.08B(40^o)	-	0.36	0.4
[20]	30	$B = 0.5$	0.5B(20^o)	0.5B(20^o)	0.56	0.7
[22]	59.5	$B = 2.4$	0(40^o)	0(40^o)	0.13	1.4
[35]	10	$B = 1.83$	0.82B(30^o)	1.06B(30^o)	0.41	-
This FSS	16.1	$B = 7.3$	1.1B(60^o)	1.14B(60^o)	0.65	0.062

bandwidth, low loss and proper performance near the cutoff frequency compared with other FSSs.

IV. CONCLUSION

A two-layer structure of FSS with steep roll-offs at the edges of the passband is proposed and manufactured. The sensitivities of transmission zeros and poles of the FSS to which parameters of the structure are analyzed directly by full-wave simulation. We associate the physical structures of the model with the lumped elements to construct the equivalent circuits of the proposed FSS, and the equivalent circuit is used to determine the impedance matching network. The results of the equivalent circuit and full-wave simulations can agree well, and it is shown that the above way is reliable. The prototype is fabricated and measured. Because of its strong capability of clutter rejection, it is a good candidate to enhance detection function of Ku-band active radar.

REFERENCES

[1] W. Wu, K. Cui, H. Lu, T. Z. Meng, and N. Yuan, "A measured rasorber with two absorptive bands," *Radioengineering*, vol. 26, no. 4, pp. 979–983, Dec. 2017.

[2] S. M. A. M. H. Abadi, M. Li, and N. Behdad, "Harmonic-suppressed miniaturized-element frequency selective surfaces with higher order bandpass responses," *IEEE Trans. Antennas Propag.*, vol. 62, no. 5, pp. 2562–2571, May 2014.

[3] M. Gao, S. M. A. M. H. Abadi, and N. Behdad, "A dual-band, inductively coupled miniaturized-element frequency selective surface with higher order bandpass response," *IEEE Trans. Antennas Propag.*, vol. 64, no. 8, pp. 3729–3734, Aug. 2016.

[4] B. A. Munk, *Frequency Selective Surfaces: Theory and Design*. New York, NY, USA: Wiley, 2000.

[5] N. Behdad, "A second-order band-pass frequency selective surface using nonresonant subwavelength periodic structures," *Microw. Opt. Technol. Lett.*, vol. 50, no. 6, pp. 1639–1643, 2008.

[6] D. S. Lockyer, J. C. Vardaxoglou, and R. A. Simpkin, "Complementary frequency selective surfaces," *IEE Proc.-Microw., Antennas Propag.*, vol. 147, no. 6, pp. 501–507, Dec. 2001.

[7] J. Romeu and Y. Rahmat-Samii, "Fractal FSS: A novel dual-band frequency selective surface," *IEEE Trans. Antennas Propag.*, vol. 48, no. 7, pp. 1097–1105, Jul. 2000.

[8] F. Bayatpur and K. Sarabandi, "Single-layer high-order miniaturized-element frequency-selective surfaces," *IEEE Trans. Microw. Theory Techn.*, vol. 56, no. 4, pp. 774–781, Apr. 2008.

[9] W. Wu, X. Liu, K. Cui, Y. Ma, and Y. Yuan, "An ultrathin and polarization-insensitive frequency selective surface at Ka-band," *IEEE Antennas Wireless Propag. Lett.*, vol. 17, no. 1, pp. 74–77, Jan. 2018.

[10] J. P. Gianvittorio, J. Romeu, S. Blanch, and Y. Rahmat-Samii, "Self-similar prefractal frequency selective surfaces for multiband and dual-polarized applications," *IEEE Trans. Antennas Propag.*, vol. 51, no. 11, pp. 3088–3096, Nov. 2003.

[11] D. H. Werner and D. Lee, "Design of dual-polarised multiband frequency selective surfaces using fractal elements," *Electron. Lett.*, vol. 36, no. 6, pp. 487–488, Mar. 2000.

[12] L. Bing-yuan, X. Zheng-Hui, L. Wei-Ming, and R. Wu, "Ultra-wideband frequency selective surface at K and Ka band," in *Proc. IEEE Int. Conf. Microw. Technol. Comput. Electromagn.*, Aug. 2013, pp. 55–57.

[13] D. Feng, Z. Shenquan, D. Fan, and W. Dongdong, "A n-order ultra wide-band frequency selective surface," in *Proc. Int. Symp. Antennas, Propag. Em Theory*, Oct. 2016, pp. 648–651.

[14] N. Xu, J. Gao, J. Zhao, and X. Feng, "A novel wideband, low-profile and second-order miniaturized band-pass frequency selective surfaces," *AIP Adv.*, vol. 5, no. 7, pp. 55–57, Jul. 2013.

[15] H. Zhou *et al.*, "Ultra-wideband frequency selective surface," *Electron. Lett.*, vol. 7, no. 1, pp. 11–13, Jan. 2012.

[16] N. Behdad, M. Al-Joumayly, and M. Salehi, "A low-profile third-order bandpass frequency selective surface," *IEEE Trans. Antennas Propag.*, vol. 57, no. 2, pp. 460–466, Feb. 2009.

[17] S. M. A. M. H. Abadi and N. Behdad, "Wideband linear-to-circular polarization converters based on miniaturized-element frequency selective surfaces," *IEEE Trans. Antennas Propag.*, vol. 64, no. 2, pp. 525–534, Feb. 2016.

[18] A. K. Rashid and Z. Shen, "A novel band-reject frequency selective surface with pseudo-elliptic response," *IEEE Trans. Antennas Propag.*, vol. 58, no. 4, pp. 1220–1226, Apr. 2010.

[19] B. Li and Z. Shen, "Three-dimensional bandpass frequency-selective structures with multiple transmission zeros," *IEEE Trans. Microw. Theory Techn.*, vol. 61, no. 10, pp. 3578–3589, Oct. 2013.

[20] G. Q. Luo, W. Hong, Q. H. Lai, K. Wu, and L. L. Sun, "Design and experimental verification of compact frequency-selective surface with quasi-elliptic bandpass response," *IEEE Trans. Microw. Theory Techn.*, vol. 55, no. 12, pp. 2481–2487, Dec. 2007.

[21] G. Q. Luo, W. Hong, Q. H. Lai, and L. L. Sun, "Frequency-selective surfaces with two sharp sidebands realised by cascading and shunting substrate integrated waveguide cavities," *IET Microw., Antennas Propag.*, vol. 2, no. 1, pp. 23–27, Feb. 2008.

[22] D. S. Wang, P. Zhao, and C. H. Chan, "Design and analysis of a high-selectivity frequency-selective surface at 60 GHz," *IEEE Trans. Microw. Theory Techn.*, vol. 64, no. 6, pp. 1694–1703, Jun. 2016.

[23] M. Li and N. Behdad, "A third-order bandpass frequency selective surface with a tunable transmission null," *IEEE Trans. Antennas Propag.*, vol. 60, no. 4, pp. 2109–2113, Apr. 2012.

[24] D. Wang, W. Che, Y. Chang, K.-S. Chin, and Y. L. Chow, "Combined-element frequency selective surfaces with multiple transmission poles and zeros," *IET Microw., Antennas Propag.*, vol. 8, no. 3, pp. 186–193, Feb. 2014.

[25] B. Li and Z. Shen, "Synthesis of quasi-elliptic bandpass frequency-selective surface using cascaded loop arrays," *IEEE Trans. Antennas Propag.*, vol. 61, no. 6, pp. 3053–3059, Jun. 2013.

[26] A. Abbaspour-Tamijani, K. Sarabandi, and G. M. Rebeiz, "Antenna-filter-antenna arrays as a class of bandpass frequency-selective surfaces," *IEEE Trans. Microw. Theory Techn.*, vol. 52, no. 8, pp. 1781–1789, Aug. 2004.

[27] S. Narayan, K. Prasad, R. U. Nair, and R. M. Jha, "A novel EM analysis of double-layered thick FSS based on MM-GSM technique for radome applications," *Prog. Electromagn. Res.*, vol. 28, pp. 53–62, Nov. 2012.

[28] F. Costa, A. Monorchio, and G. Manara, "Efficient analysis of frequency-selective surfaces by a simple equivalent-circuit model," *IEEE Antennas Propag. Mag.*, vol. 54, no. 4, pp. 35–48, Aug. 2012.

[29] Y. C. Chung, K.-W. Lee, I.-P. Hong, M.-G. Lee, H.-J. Chun, and J.-G. Yook, "Simple prediction of FSS radome transmission characteristics using an FSS equivalent circuit model," *IEICE Electron. Express*, vol. 5, no. 2, pp. 89–95, 2011.

[30] D. Ferreira, R. F. da Silva Caldeirinha, I. Cuiñas, T. R. Fernandes, "Tunable square slot FSS EC modelling and optimisation," *IET Microw. Antennas Propag.*, vol. 11, no. 5, pp. 737–742, Apr. 2017.

[31] N. Liu, X. Sheng, C. Zhang, J. Fan, and D. Guo, "A design method for synthesizing wideband band-stop FSS via its equivalent circuit model," *IEEE Antennas Wireless Propag. Lett.*, vol. 16, pp. 2721–2725, 2017.

[32] K.-W. Lee, Y.-R. Jeong, I.-P. Hong, M.-G. Lee, H.-J. Chun, and J.-G. Yook, "Simple design method of FSS radome analysis using equivalent circuit model," *IEICE Electron. Express*, vol. 8, no. 23, pp. 2002–2009, 2011.
[33] S. Ghosh and K. V. Srivastava, "An equivalent circuit model of FSS-based metamaterial absorber using coupled line theory," *IEEE Antennas Wireless Propag. Lett.*, vol. 14, pp. 511–514, 2015.
[34] S. B. Savia and E. A. Parker, "Equivalent circuit model for superdense linear dipole FSS," *IEE Proc.-Microw., Antennas Propag.*, vol. 150, no. 1, pp. 37–42, Feb. 2003.
[35] J. Yuan, S. Liu, B. Bian, X. Kong, H. Zhang, and S. Wang, "A novel high-selective bandpass frequency selective surface with multiple transmission zeros," *J. Electromagn. Waves Appl.*, vol. 28, no. 17, pp. 2197–2209, 2014.

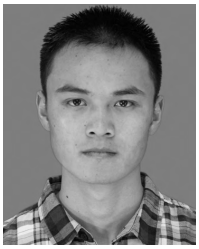

YUHONG MA was born in 1995. He received the B.S. degree in electronic science and technology from the National University of Defense Technology, Changsha, China, in 2017, where he is currently pursuing the M.S. degree with the College of Electronic Science and Engineering. His current research interests involve RF/microwave circuits, ultra-wide-band technology, microstrip antennas, and filters.

WEIWEI WU was born in 1981. She received the M.S. and Ph.D. degrees in electronic science and technology from the National University of Defense Technology, Changsha, China, in 2008 and 2011, respectively. She is currently a Teacher with the College of Electronic Science and Engineering, National University of Defense Technology. Her research interests include antennas design and wave propagation.

YE YUAN was born in 1994. He received the B.S. degree in electronic science and technology from the Nanjing University of Aeronautics and Astronautics in 2016. He is currently pursuing the M.S. degree with the College of Electronic Science and Engineering, National University of Defense Technology, Changsha, China. His research interests include passive microwave circuits design and wireless communication.

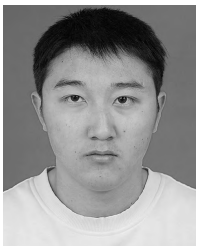

WENTAO YUAN was born in 1990. He received the B.S. degree in computer science and technology from Anhui Normal University in 2016. He is currently pursuing the M.S. degree with the College of Electronic Science and Engineering, National University of Defense Technology, Changsha, China. His research interests include passive microwave circuits design and wireless communication.

NAICHANG YUAN was born in 1965. He received the M.S. and Ph.D. degrees in electronic science and technology from the University Science and Technology of China in 1991 and 1994, respectively. He is currently a Professor with the College of Electronic Science and Engineering, National University of Defense Technology, Changsha, China. His research interests include microwave circuits design, wireless communication, and wave propagation.